Cancer Letters 449 (2019) 125–134

Contents lists available at ScienceDirect

Cancer Letters

journal homepage: www.elsevier.com/locate/canlet

Original Articles

Anterior Gradient-2 monoclonal antibody inhibits lung cancer growth and metastasis by upregulating p53 pathway and without exerting any toxicological effects: A preclinical study

Hema Negi[a,1], Siva Bharath Merugu[a,1], Hitesh Bhagavanbhai Mangukiya[a], Zheqi Li[b], Bingjie Zhou[a], Qudsia Sehar[a], Suchitra Kamle[c], Fakhar-un-Nisa Yunus[a], Dhahiri Saidi Mashausi[a], Zhenghua Wu[a,**], Dawei Li[a,d,*]

[a] School of Pharmacy, Shanghai Jiao Tong University, Shanghai, China
[b] Department of Molecular Pharmacology and Chemical Biology, School of Medicine, University of Pittsburgh, PA, USA
[c] Division of Molecular Microbiology and Immunology, Brown University, Providence, RI, USA
[d] Engineering Research Center of Cell and Therapeutic Antibody of Ministry of Education, Shanghai Jiao Tong University, China

ARTICLE INFO

Keywords:
mAb18A4
Anti-AGR2 monoclonal antibody
NSCLC
Angiogenesis
MAPK
p53
Toxicology

ABSTRACT

Increased drug resistance and acute side effects on normal organs are the major disadvantages of traditional cancer chemotherapy and radiotherapy. This has increased the focus on targeted therapeutic strategies such as monoclonal antibody-based cancer therapies. The major advantage of antibody-based therapies is the specific inhibition of cancer-related targets, with reduced off-target side effects. Anterior gradient-2 (AGR2) is a pro-metastatic and proangiogenic tumor marker that is overexpressed in multiple cancers. Therefore, anti-AGR2 antibodies may be potential therapeutic agents for treating different cancers. In the present study, we examined a novel anti-AGR2 monoclonal antibody mAb18A4 and found that this antibody inhibited lung cancer progression and metastasis without exerting any adverse side effects on the major organs and blood in mice. Moreover, we found that mAb18A4 activated p53 pathway and attenuated ERK1/2–MAPK pathway. Furthermore, mAb18A4-treated cancer cell lines showed attenuated proliferation and colony formation, enhanced apoptosis, increased p53 expression, and reduced phosphorylated ERK1/2 expression. Treatment with mAb18A4 significantly reduced tumor size and suppressed tumor metastasis in and increased the survival of different xenograft tumor models. In addition, mAb18A4 potently suppressed AGR2-induced angiogenesis. Results of pharmacokinetic and toxicological analyses confirmed the safety of mAb18A4 as an antitumor treatment.

1. Introduction

Anterior gradient-2 (AGR2) is a proangiogenic and protein belonging to protein disulfide isomerase family and resides in the endoplasmic reticulum (ER) [1]. AGR2 is overexpressed in multiple cancers, including lung, breast, prostate, ovarian, gastric, and pancreatic cancers and in esophageal and nasopharyngeal carcinomas [2–4]. Similar to an ER chaperone, AGR2 shows tumorigenic properties by promoting tumor cell survival, migration, and invasion; drug resistance; angiogenesis; and metastasis [3,5–9]. Elevated AGR2 expression is associated with the poor survival of patients with breast and lung cancers [10–12]. In the tumor microenvironment, AGR2 plays a crucial role by engaging in a cross-talk with growth factors, thereby enhancing their function [13–16]. AGR2 interferes with cell survival and metastasis pathways by modulating survivin, cyclin D1, cathepsin B and D, CD147, and epidermal growth factor receptor (EGFR) levels. Moreover, AGR2 promotes malignant transformation by interacting with C4.4A and DAG-1 proteins [17]. Furthermore, AGR2 inhibits the function of p53, a tumor suppressor protein [18,19]. Besides its role in carcinogenesis, AGR2 is involved in limb and tail regeneration in *Xenopus laevis* tadpoles, and extracellular AGR2 plays a prominent role in wound healing [20]. AGR2 expression is high in mucus-secreting cells and endocrine organs, including the small intestine, colon, lungs, and stomach [2,21]. Moreover, AGR2 is essential for mucin production in the intestine [22].

* Corresponding author.School of Pharmacy, Shanghai Jiao Tong University, Shanghai, 200240, China.
** Co-corresponding author. School of Pharmacy, Shanghai Jiao Tong University, Shanghai, 200240, China.
E-mail addresses: wuzhenghua@sjtu.edu.cn (Z. Wu), daweili@sjtu.edu.cn (D. Li).
[1] H. Negi and S.B. Merugu contributed equally to this work.

https://doi.org/10.1016/j.canlet.2019.01.025
Received 18 October 2018; Received in revised form 27 December 2018; Accepted 21 January 2019

Lung cancer accounts for the highest mortality rate worldwide and is incurable [23]. Patients with non-small cell lung cancer (NSCLC) show poor prognosis because available therapies are ineffective against lung adenocarcinomas containing mutations in genes such as *EGFR*, *KRAS*, *BRAF*, and *PIK3CA* [24–26]. Therefore, targeted therapy has gained considerable attention for lung cancer treatment. Gefitinib and erlotinib are the first-line chemotherapy drugs for treating NSCLC. Bevacizumab is the first recombinant human monoclonal antibody that is widely used for treating intermediate- and advance-stage NSCLCs [27]. AGR2 is highly overexpressed in lung adenocarcinoma and is associated with poor patient survival [11,28]. Moreover, AGR2 is associated with *EGFR* mutations in lung adenocarcinomas [29]. Together, these findings indicate the potential of AGR2 as a target for treating lung cancer.

Because AGR2 is a novel therapeutic target, we designed and developed a monoclonal antibody called mAb18A4 against human AGR2 [30]. In the present study, we found that mAb18A4 exerted antitumor, angiostatic, and antimetastatic effects and was non-toxic in mice. Moreover, we found that mAb18A4 upregulated p53 pathway and downregulated ERK1/2–MAPK pathway.

2. Materials and methods

2.1. Cell culture

H460, A549, and B16F10 cells were cultured in Dulbecco's modified Eagle's medium (DMEM), and 4T1 cells were cultured in Roswell Park Memorial Institute 1640 medium. Both the media were supplemented with 10% fetal bovine serum and 1% penicillin/streptomycin, and the cells were incubated at 37 °C in a humidified incubator with 5% CO_2.

2.2. Wound-healing assay

The cells were seeded in six-well plates and were grown to approximately 100% confluency. Next, the cells were starved for 24 h by culturing in a serum-free medium. Wounds were created in the cell monolayers in each well by using a pipette tip, followed by treatment with mAb18A4. Images were captured at 0 and 48 h after wound induction. The distance migrated by the cells into the wound was measured using IMAGE PRO PLUS software.

2.3. Trypan blue dye exclusion assay

The cells were seeded (density, 10,000 cells/well) in a six-well plate. After 24 h, the cells were treated with mAb18A4 and were incubated for 48 h. At the end of the experiment, the cells were digested with trypsin and were counted using trypan blue dye.

2.4. MTT assay

The cells (density, 5000 cells/well) were seeded in 96-well plates. After 24 h, the cells were treated with mAb18A4 for 48 h, followed by incubation with MTT (500 μg/ml) for 4 h. Absorbance was measured at 570 nm by using a microplate reader. Cell survival percentage was calculated using the ratio of reported value and control value.

2.5. Western blotting analysis

Cells and tumor tissues were lysed using NP-40 lysis buffer with protease inhibitor (Sigma, USA). Proteins were separated by SDS-PAGE and immunoblotted for antibody detection with p53 (Proteintech, USA, #10422-1-AP), p44/p42 MAPK (137F5, Cell Signal Technology, USA, #4695), phosphor-p44/42 MAPK (T202/Y204, 20G11,Cell Signal Technology,USA, #9101) and p21 Waf1/Cip1 (12D1, Cell Signal Technology, USA, #2947) antibodies.

β-actin (Santa Cruz, USA, sc-47778) and GAPDH (Proteintech, USA, # 60004-1-Ig) were used as loading controls.

2.6. Colony formation assay

The cells (density, 5000 cells/well) were seeded in a six-well plate and were treated with mAb18A4. Colonies formed after 14 days were stained with 0.5% crystal violet. Quantification analysis was performed by counting the number of colonies formed.

2.7. Xenograft tumor models

Animal study procedures were approved by the Institutional Animal Care and Use Committee of Shanghai Jiao Tong University. Tumor cells (density, 5×10^6 cells) were subcutaneously inoculated into the flanks of 6-week-old BALB/c nude mice, and the mice were divided into two groups, namely, control and treatment groups. The mice in the treatment group (n = 5) were intraperitoneally injected with 16 mg/kg mAb18A4 biweekly from day 2 after the tumor cell inoculation. Tumor growth was monitored by measuring tumor volume ($1/2 \times \text{length} \times \text{width}^2$) on indicated days. The mice were sacrificed at the end of the experiment. Their tumors and organs were harvested, fixed with 4% paraformaldehyde, embedded in paraffin, and sectioned into 10-μm-thick sections. These sections were used for performing hematoxylin-eosin (H&E) staining, immunofluorescence (IF) analysis, and immunohistochemical (IHC) analysis. For angiogenesis analysis, the mice were inoculated with the tumor cells and were treated with mAb18A4 in the same manner as that described above. At the end of the experiment, the mice were sacrificed, their tumors were exposed, and the number of blood vessels surrounding the tumors was determined.

2.8. Orthotopic 4T1 breast cancer model

The 4T1 cells (density, 5×10^5 cells) were inoculated into the #4 mammary fat pad of isogenic BALB/c nude mice. Next, the mice were treated with mAb18A4 biweekly from day 2 after the tumor cell inoculation. On day 21, the mice were sacrificed and tumor metastasis to the #9 fat pad, lungs, and liver was analyzed. The mouse organs were harvested, embedded in paraffin, sectioned into 10-μm-thick sections, and analyzed by performing H&E staining.

2.9. B16F10 lung metastasis model

The B16F10 cells (density, 20×10^4 cells) were inoculated into the mice through the tail vein, and the mice were treated with mAb18A4 twice a week from day 2 after the tumor cell inoculation. The mice were sacrificed on day 19, and their lungs were removed to visualize tumors. After harvesting, the mouse lungs were fixed in 4% paraformaldehyde, embedded in paraffin, sectioned into 10-μm-thick sections, and analyzed by performing H&E staining.

2.10. Survival rate determination

The mice were inoculated with the B16F10 cells (density, 20 × 104 cells) through the tail vein and were divided into two groups, namely, control and treatment groups. The mice in the treatment group were treated with mAb18A4 twice a week from day 2 after the tumor cell inoculation. The experiment was repeated until the last mouse in either one of the two groups was dead.

2.11. Aortic ring assay

The angiostatic effect of mAb18A4 was determined by performing a mouse aortic ring assay, as described previously [31]. Mouse explants were incubated with AGR2 and mAb18A4 and were examined every day under a microscope (LIFE Technologies, USA).

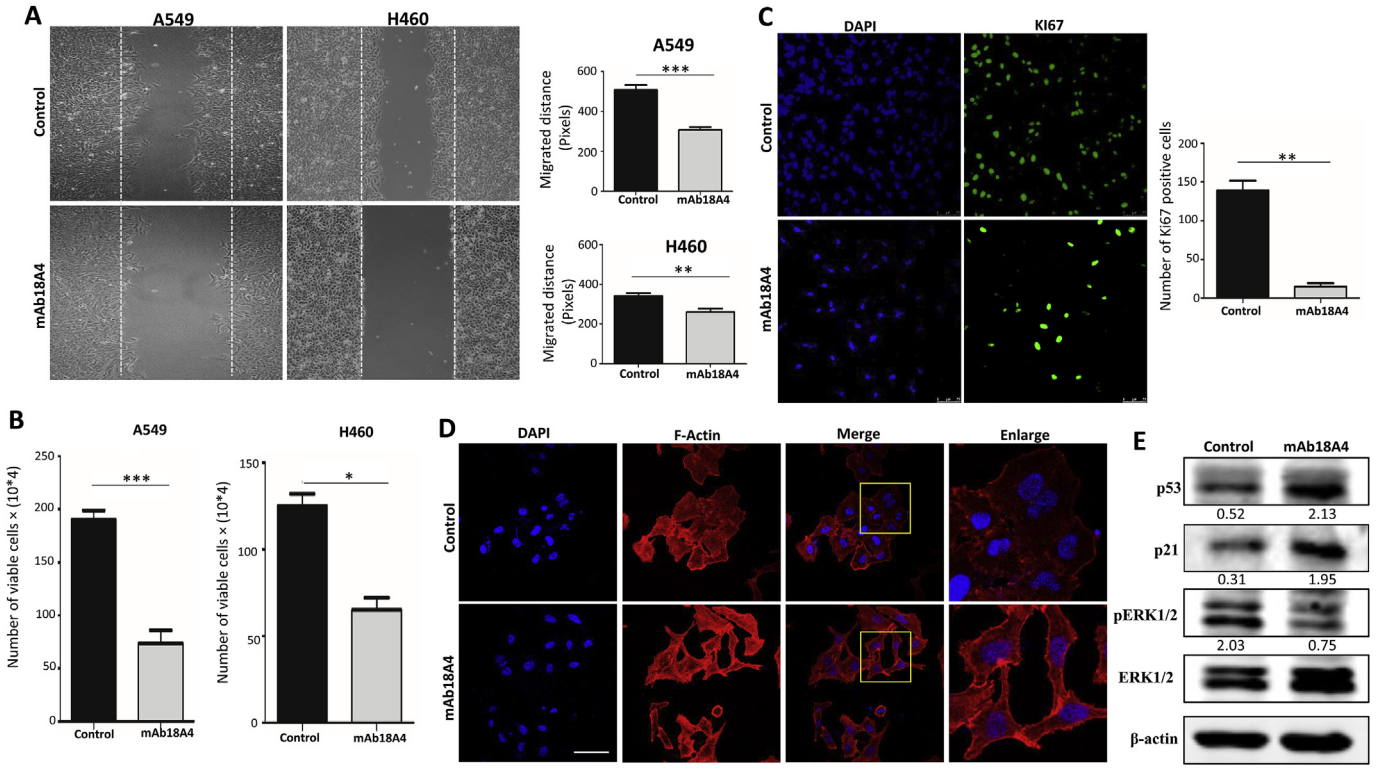

Fig. 1. mAb18A4 inhibits migration, suppresses proliferation, disrupts cellular morphology and reduces phosphorylation of ERK *invitro*. A) Serum starved NSCLC cells A549 & H460 cells were treated with mAb18A4 for 48 h and scratch wound healing assay was performed. The anti-AGR2 antibody treatment inhibited migration significantly. (B) In tryphan blue assay, cells were treated with mAb18A4 for 48 h. The viable cells were counted and shown as a bar graph with SD from three independent experiments. (C) Representative pictures of Ki67 staining. Nuclei were counter stained with DAPI (blue). mAb18A4 significantly reduced proliferation as compared to control. Scale bar, 75 μm. (D) A549 cells were treated with mAb18A4 for 48 h; cells were then stained with Alexa fluor 594 phalloidin for F-actin. The treated cells showed disrupted morphology and cytoskeleton organization. Scale bar, 50 μm. (E) H460 cells were treated with mAb18A4 for 48 h and lysates were subjected to western blotting.
Signals were quantified with Graph Pad Prism and Image J. *, ** and *** indicate $P < 0.05$, $P < 0.02$, and $P < 0.001$ respectively, as determined by an unpaired 2-tail student t-test from three treatments. (For interpretation of the references to colour in this figure legend, the reader is referred to the Web version of this article.)

2.12. Immunofluorescence analysis

The cells were grown on coverslips, fixed with 4% formaldehyde for 15 min, and blocked with goat serum for 30 min. Next, the coverslips were incubated with an anti-Ki67 (ab15580, Abcam, USA) antibody for 2 h or with TRITC-conjugated phalloidin (FAK100, Milipore, USA) for 1 h, followed by incubation with Dylight 594- or Dylight 488-conjugated anti-rabbit secondary antibody (MultiSciences Biotech). Nuclei were stained with DAPI (Invitrogen). Images were obtained using a laser scanning confocal microscope (Leica). Mouse tissues were embedded in paraffin, sectioned into 10-μm-thick sections, and fixed in 4% paraformaldehyde. Next, the sections were blocked with goat serum for 1 h, followed by overnight incubation with the anti-Ki67 antibody at 4 °C. The sections were then washed with PBS and incubated with the anti-rabbit Dylight 594-conjugated secondary antibody. Nuclei were counterstained using DAPI. Images were obtained using a laser scanning confocal microscope.

2.13. Immunohistochemical analysis

Mouse tumor and organ tissues were embedded in paraffin and were sectioned into 10-μm-thick sections. IHC analysis was performed as described previously [20] by using antibodies against p53, phosphorylated p44/42 MAPK, α-SMA (Cell Signal Technology, USA, #19245), CD31 (Novus Biologicals, NB100-2284), VEGF (abcam, USA, ab39250), BCL-2 (ABclonal, A0208), BAX (ABclonal, A12009), AGR2 (Proteintech, USA, 12275-1-AP) and MUC2 (GServicebio, China, GB11344). Quantification of the data was done by IMAGE J software.

2.14. Pharmacokinetic analysis

Four C57/BL6 mice were intravenously injected with a single dose of mAb18A4 (16 mg/kg). Serum samples were collected from the mice at indicated time points (30 min, 2 h, 6 h, 1 day, 2 days, 3 days, 5 days, and 7 days), and antibody concentration in the serum samples was determined by performing ELISA.

2.15. Toxicology analysis

The C57/BL6 mice were intravenously injected with 16 mg/kg mAb18A4 biweekly for 5 weeks. At the end of the experiment, mouse blood samples were collected by performing cardiac puncture and mouse organs were harvested. Hematological and serum biochemical analyses were conducted commercially at G-Service Bio (Shanghai, China). The mouse organs were fixed with 4% formaldehyde, embedded in paraffin, sectioned into 10-μm-thick sections, and were analyzed by performing H&E staining.

2.16. Statistical analysis

All values are expressed as mean ± standard deviation, unless otherwise indicated. Graphs were plotted using GraphPad Prism software. Differences between the groups were compared used a two-tailed unpaired Student's *t*-test. P values and sample sizes are described in figure legends.

3. Results

3.1. mAb18A4 inhibits tumor growth and metastasis in vitro and disrupts tumor cell morphology and cytoskeleton organization

First, we conducted *in vitro* experiments to determine the antitumor efficacy of mAb18A4 against NSCLC cell lines A549 and H460 that show high AGR2 expression. Both the NSCLC cell lines were treated with the anti-AGR2 antibody mAb18A4, and wound-healing assays were performed. We observed that the number of cells migrating into the wounds was significantly lower among the mAb18A4-treated cells than among control cells (Fig. 1A). In the trypan blue dye exclusion assay, the serum-starved cells were treated with mAb18A4 for 48 h under the indicated conditions and were counted (Fig. 1B). Ki67 staining (Fig. 1C) and the MTT assay (Supplementary Fig. S1B) were performed to evaluate tumor cell proliferation. We observed that the mAb18A4-treated cells showed drastically lower proliferation than the control cells. A similar trend was observed by performing the colony formation assay (Supplementary Fig. S1A). Together, these results indicate that mAb18A4 reduces the migration, proliferation, and viability of the NSCLC cells.

The actin cytoskeleton plays a crucial role in cell adhesion, migration, morphogenesis, and invasion [32]. We examined whether mAb18A4 treatment affected motility changes associated with the morphology of and actin cytoskeleton in NSCLC cells. The A549 cells were stained with TRITC-conjugated phalloidin to detect F-actin (Fig. 1D). We observed that the mAb18A4-treated cells were elongated and retracted and showed cytoskeleton remodeling, whereas control cells showed a round morphology which is consistent with previous litrature [33]. Cell–cell junctions were not distinguishable in the control cells, whereas large intracellular gaps were observed in the mAb18A4-treated cells. These findings suggest that the anti-AGR2 antibody mAb18A4 disrupts cell morphology and F-actin cytoskeleton.

The MAPK signaling pathway regulates cell migration, proliferation, apoptosis, and survival [34], and AGR2 is involved in these processes [35]. Therefore, we examined whether the mAb18A4-treated AGR2-expressing cancer cells showed changes in phosphorylated ERK1/2, p53, and p21 levels. Results of the western blotting analysis showed reduced phosphorylated ERK1/2 expression levels and increased p53 and p21 expression levels in the mAb18A4-treated cells (Fig. 1E). We also analyzed the effect of 48-h mAb18A4 treatment on normal breast (MCF7-10A) cells and human embryonic kidney (293T) cells (Supplementary Fig. S1C) and observed no significant change in the proliferation of these cells, as evaluated by performing the MTT assay.

Before determining the efficacy of mAb18A4, we examined AGR2 expression levels in different cancer types [36,37]. We found that AGR2 expression was comparatively higher in lung cancer than that in other cancers, thus making it a good target for assessing the effect of mAb18A4 (Supplementary Fig. S2).

3.2. mAb18A4 inhibits NSCLC xenograft tumor growth and reduces tumor weight

Next, we evaluated the effect of mAb18A4 in different lung adenocarcinoma xenograft tumor models (A549 and H460 NSCLC xenograft tumor models) because AGR2 is highly expressed in lung adenocarcinomas and is associated with poor prognosis [11]. The xenograft tumor models were generated by subcutaneously inoculating 5×10^6 tumor cells into nude mice. The mice were divided into control and treatment groups. The mice in the treatment group were injected with 16 mg/kg mAb18A4 biweekly from day 2 after the tumor cell inoculation. The efficacy of mAb18A4 against tumor growth was evaluated by measuring tumor volume twice a week. We observed that mAb18A4 significantly inhibited tumor growth in the xenograft tumor models ($P < 0.001$ and $P < 0.05$ for the A549 and H460 NSCLC xenograft tumor models, respectively; Fig. 2A). Moreover, mAb18A4 significantly reduced tumor weights in both the xenograft tumor models (Fig. 2B). In addition, the mAb18A4-treated mice did not show appetite loss and body weight alteration during the treatment period, indicating that the mAb18A4 dose used in the present study was well tolerated by the mice (data not shown).

3.3. mAb18A4 suppresses tumor cell proliferation, induces tumor cell apoptosis, triggers p53 pathway, and attenuates ERK1/2–MAPK pathway

Tumors were harvested from the mice at the end of the experiment for performing IHC and IF analyses. H&E staining detected multiple necrotic areas in tumors isolated from the mAb18A4-treated mice compared with those isolated from the control mice (Supplementary Fig. S3A). Interestingly, the level of the proliferation marker Ki67 was significantly reduced in the tumors isolated from the mAb18A4-treated mice (Fig. 2C). Moreover, the shape and number of tumor cells was notably reduced in the tumors isolated from the mAb18A4-treated mice.

Next, we examined the expression of apoptosis markers in the tumor tissues isolated from the mice and found that BAX expression was increased and BCL2 expression was decreased in the tumors isolated from the mAb18A4-treated mice, indicating that mAb18A4 induced tumor cell apoptosis *in vivo* (Fig. 2D). AGR2 inhibits p53; therefore, we stained the xenograft tumor tissues with the anti-p53 antibody and observed increased p53 expression in the tumor tissues isolated from the mAb18A4-treated mice (Fig. 2D). Furthermore, we observed that mAb18A4 reduced ERK1/2 phosphorylation (Fig. 2D), indicating that this antibody acted through the ERK1/2–MAPK pathway. Results of the western blotting analysis showed the same trend for p53, phosphorylated ERK1/2, and p21 levels in the lysates of tumors isolated from the mAb18A4-treated mice (Fig. 2E).

Next, we evaluated the effect of mAb18A4 on α-SMA level because AGR2 exerts a paracrine effect on fibroblasts [13]. Furthermore, we found that AGR2 expression levels were significantly reduced in the tumors isolated from the mAb18A4-treated mice (Supplementary Fig. S3B). Next, we assessed the binding and distribution of mAb18A4 in the tumor tissues of the mice (Supplementary Fig. S3C). Results of the IHC analysis of the tumor tissues isolated from the mice treated with mAb18A4 showed that this antibody was localized in the necrotic areas in the tumor tissues.

3.4. mAb18A4 inhibits AGR2-induced angiogenesis

We recently found that AGR2 binds to VEGF and bFGF and enhances their functions, thus promoting angiogenesis [14]. Jia et al. [8] also reported that AGR2 is a proangiogenic protein and suppresses the activity of bevacizumab, an FDA-approved anti-VEGF antibody. Therefore, we examined whether mAb18A4 inhibited AGR2-induced angiogenesis. Notably, the tumors isolated from the control mice showed numerous blood vessels compared with the tumors isolated from the mAb18A4-treated mice (Fig. 3A). Results of the IF and IHC analyses showed a marked reduction in tumor vessel density, as indicated by a decrease in CD31 (Fig. 3B) and VEGF (Fig. 3C) staining, respectively, in the tumors isolated from the mAb18A4-treated mice compared with that in the tumors isolated from the control mice. Next, we performed *ex vivo* mouse aortic ring assay to examine the effect of mAb18A4 on angiogenesis and observed that mAb18A4 inhibited AGR2-induced angiogenesis by suppressing the formation of neo-endothelial vessels (Fig. 3D). Collectively, these results indicate that mAb18A4 disrupts tumor vasculature and inhibits AGR2-induced angiogenesis.

3.5. mAb18A4 inhibits tumor metastasis and prolongs survival

Tumor cells undergo proliferation, migration, invasion, and angiogenesis to promote tumor metastasis, and AGR2 modulates these processes in various cancer types [35]. Moreover, AGR2 promotes tumor

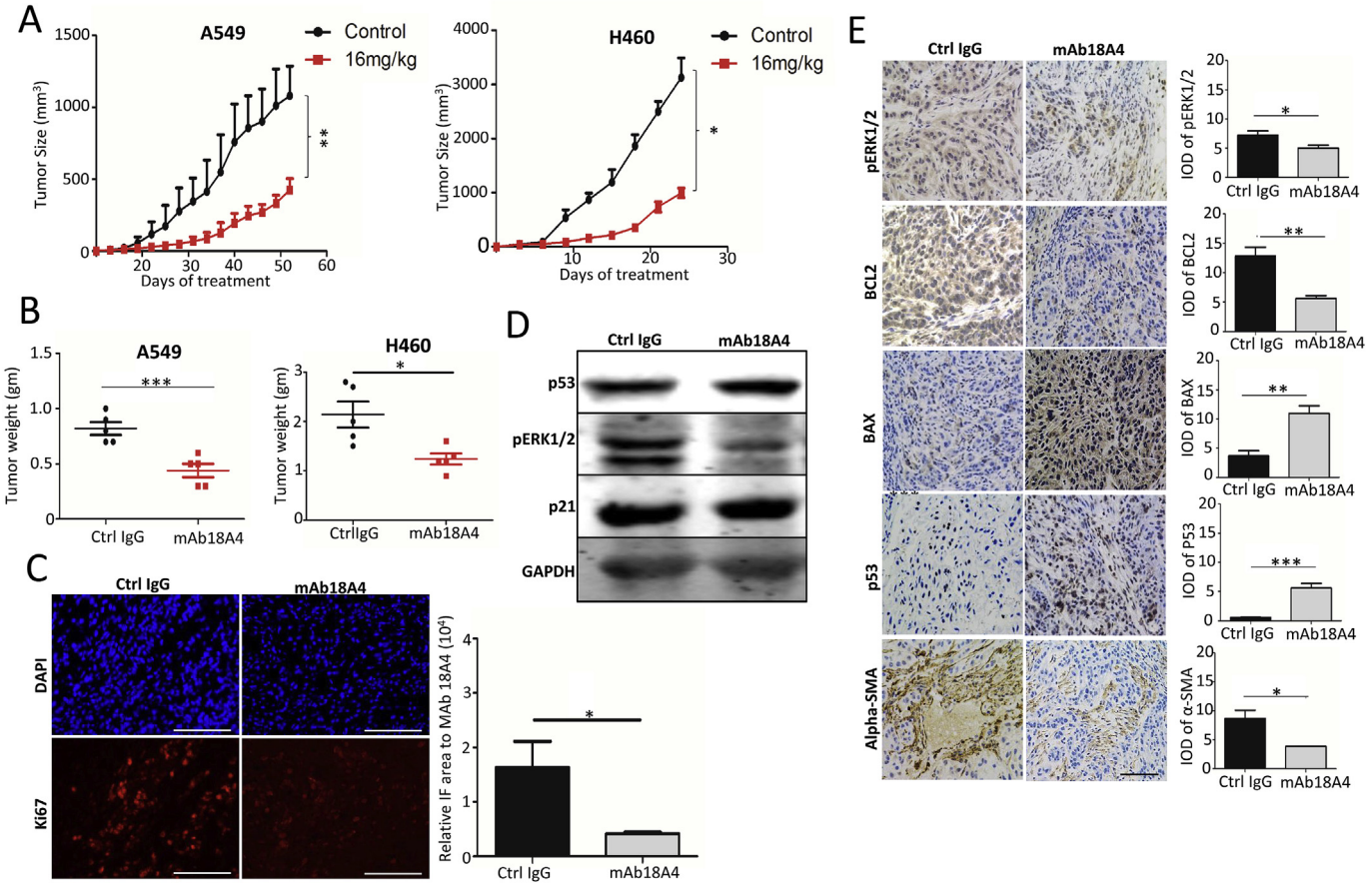

Fig. 2. mAb18A4 inhibits xenograft tumor growth, reduces proliferation, induces apoptosis, and attenuates MAPK Pathway in NSCLC Tumors. (A) The efficacy of mAb18A4 was examined in A549 and H460 xenograft models. The tumors were treated with 20 mg/kg mAb18A4 antibody, twice a week. Data shown as mean ± SEM (n = 5) quantified using GraphPad Prism. (B) Shown are the bar graphs of excised tumor weight. mAb18A4 treatment led to significant reduction in tumor weight due to its necrotic activity. (C) Representative pictures of immunofluorescence staining of mAb18A4 treated A549 tumors. mAb18A4 treatment reduced cell proliferation (Ki67) significantly. Nuclei were counterstained with DAPI (blue). (D) The frozen sections of H460 tumors (n = 5) were lysed, the lysates were mixed and subjected to Western blotting. (E) Representative immunohistochemistry pictures of mAb18A4 treated tumors showing induced apoptosis (BAX, BCL2), and increased p53 expression. Also, mAb18A4 treatment reduced phosphorylated MAPK (ERK1/2) expression and infiltrating fibroblasts (alpha-SMA). The bars represent each sample performed in triplicate, and the error bars indicate mean ± SD (n = 3). Histogram represents the integrated optical density (IOD) and relative positive area (Ki67).Signals were quantified with Image J. *, ** and *** indicate P < 0.05, P < 0.02, and P < 0.001 respectively, as determined by an unpaired 2-tail student t-test. (For interpretation of the references to colour in this figure legend, the reader is referred to the Web version of this article.)

colonization at distant sites by regulating the cell adhesion rates of detached tumor cells; furthermore, it functions as a prometastatic protein [3,38–40].

To date, not many studies have focused on the use of anti-AGR2 antibodies as a targeted therapy for cancer. In the present study, we determined the anti-metastatic activity of mAb18A4 by using the experimental model of pulmonary melanoma metastasis (B16F10 lung metastasis model) [41]. The mice were divided into two groups, i.e., the control and treatment groups. The mice in the treatment group were intraperitoneally injected with mAb18A4 through the tail vein twice a week from day 2 after the tumor cell inoculation. After 19 days, the mice were sacrificed, their lungs were harvested, and tumor nodules on the lung surface were counted (Fig. 4A). The lungs of the mAb18A4-treated mice showed significantly fewer tumor lesions (Fig. 4B) than those of the control mice. Moreover, a significant difference in lung weight was observed between the mAb18A4-treated and control mice (Fig. 4C). Histological analysis by performing H&E staining showed multiple melanoma lesions, with an unclear histology, in the paraffin-embedded lung tissues of the control mice and significantly few tumor lesions, with a clear histology, in the paraffin-embedded lung tissues of the mAb18A4-treated mice (Fig. 4D).

Next, we examined the efficacy of mAb18A4 by using the orthotopic breast adenocarcinoma (4T1) mouse model [42]. This mouse model was developed by inoculating the 4T1 cells into the #4 mammary pad of isogenic BALB/c nude mice. The mice were divided into control and treatment groups. The mice in the treatment group were administered 16 mg/kg mAb18A4 biweekly from day 2 after the tumor cell inoculation. We observed that mAb18A4 treatment slightly inhibited primary tumor growth but significantly inhibited secondary metastasis to the #9 mammary fat pad (Supplementary Fig. S4). Next, we harvested the major organs of the mice in the two groups and examined micrometastases in these organs. Numerous visible metastasized tumors were observed on the lung surface in the control mice, whereas few metastasized tumors were observed on the lung surface in the mAb18A4-treated mice (Fig. 4F). However, no significant metastases were detected in other organs. Next, we performed H&E staining of the lung tissues and observed tumor cell infiltration in the lungs of the control mice compared with that in the lungs of the mAb18A4-treated mice (Fig. 4G).

Because oncogenic AGR2 is associated with poor patient prognosis [4,11,12,43], we examined the effect of mAb18A4 on the survival of the mouse model of pulmonary melanoma metastasis. We found that the mAb18A4-treated mice showed significantly longer survival (29 days) than the control mice, which died by day 22 (Fig. 4E). These results are consistent with previous reports [17].

NCI—H460 cells are highly metastatic and produce spontaneous

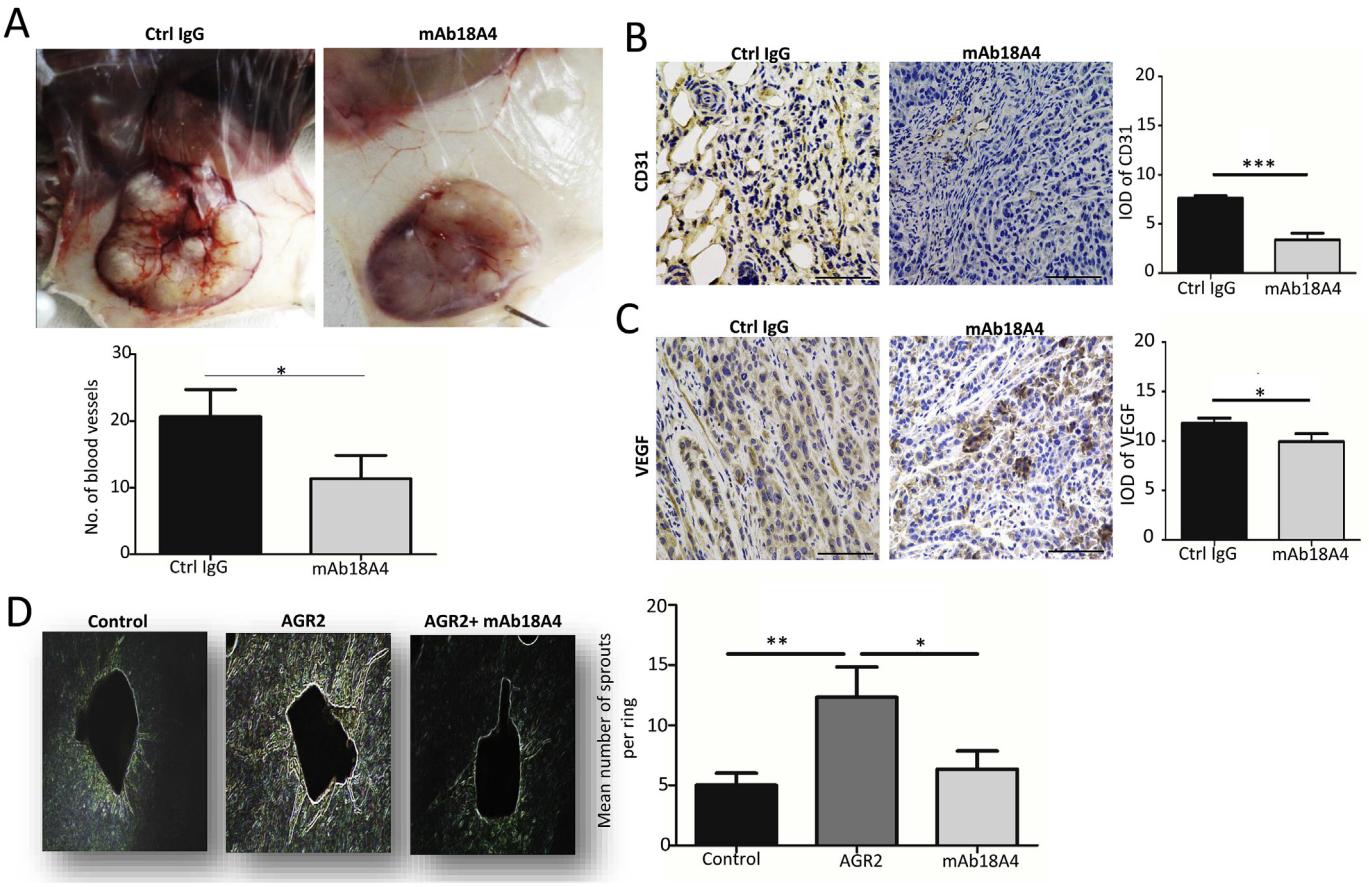

Fig. 3. mAb18A4 inhibits AGR2 induced Angiogenesis. **(A)** Representative pictures of H460 tumors showing blood vessel density. The number of blood vessels was greatly reduced in Anti-AGR2 treated group as compared to control. **(B)** Immunofluorescence staining shows mAb18A4 impedes tumor vasculature by suppressing platelet endothelial cell adhesion molecule- 1(PECAM-1) known as CD31. **(C)** Immunohistochemical staining showing vascular endothelial growth factor (VEGF). Treated tumor tissues showed lesser expression of VEGF than control. **(D)** Representative pictures of *ex vivo* mouse aortic ring assay to study angigogenesis. Aortoe were isolated from C57BL/6 mice and embedded in type 1 collagen and treated with conditions marked. Phase contrast images of aortic rings showing microvessel outgrowth. Addition of external AGR2 promotes the endothelial miscrovessel formation and the same is inhibited by mAb18A4.Statistical quantification is expressed as *, and *** indicate $P < 0.05$, and $P < 0.001$ respectively, as determined by an unpaired 2-tail student T-test. Scale bar indicates 50 μm.

metastases in 100% cases [44]. Therefore, we evaluated the effect of mAb18A4 on tumor metastases in the H460 NSCLC xenograft tumor model (Fig. 2A). Major organs were harvested from the examined mice at the end of the experiment, and histological analysis was performed. Tumor cell infiltration was observed in the lungs, colon, and small intestine of the control mice. In contrast, the mAb18A4-treated mice showed significantly less number of micrometastases in the examined organs (Fig. 4H). Together, these results indicate that mAb18A4 potently inhibits metastasis *in vivo*.

3.6. Humanized mAb18A4 does not exert adverse effect on mucin production in the intestine

Murine AGR2 is ubiquitously expressed in goblets cells and is crucial for intestinal mucus production [23]. To evaluate the adverse effect of mAb18A4 on intestinal AGR2 and MUC2, a major intestinal mucin [45], C57/BL6 mice were treated with 16 mg/kg mAb18A4 (treatment group) or IgG (control group) twice a week for 5 weeks. The colon and small intestine of the mice in the two groups were harvested at the end of experiment, and IHC analysis was performed. Results of the IHC analysis showed no decrease or change in AGR2 and MUC2 expression in both the intestine and colon of the mAb18A4-treated mice (Fig. 5A and B). Periodic acid-Schiff and Alcian blue staining showed that mAb18A4 treatment did not exert any adverse effect on heavy glycoproteins and mucus in the colon and small intestine (Fig. 4C and D). Together, these results indicate that mAb18A4 treatment does not exert any side effects on intestinal mucus production.

3.7. Pharmacokinetic and toxicology analyses of humanized mAb18A4

Pharmacokinetic (PK) and toxicology analyses of the humanized anti-AGR2 mAb18A4 were conducted using the C57/BL6 mice. In the single-dose PK study, the serum samples of the mice were collected at the designated time points and mAb18A4 concentration in the serum was measured by performing ELISA. We found that the area under curve for 16 mg/kg mAb18A4 was 1538.217 ± 325.45 μg h/ml. The mean maximum concentration of mAb18A4 in the serum was 16.7 μg/ml, and the mean half-life of mAb18A4 in the serum was > 3 days (Supplementary Table 1).

For the toxicology analysis, the mice in the treatment group were intravenously injected with 16 mg/kg mAb18A4 twice a week for 6 weeks and those in the control group were treated with IgG. At the end of the experiment, blood samples were collected from the mice through cardiac puncture for performing complete blood profile analysis and organs were harvested from the mice for performing histological analysis. No toxicity or histological abnormalities were observed in the blood (Supplementary Table 2) or major organs such as the heart, kidney, pancreas, colon, and intestine of the mAb18A4-treated mice (Fig. 6). Together, the results of the PK and toxicology analyses indicate that mAb18A4 is a safe therapeutic option for cancer therapy.

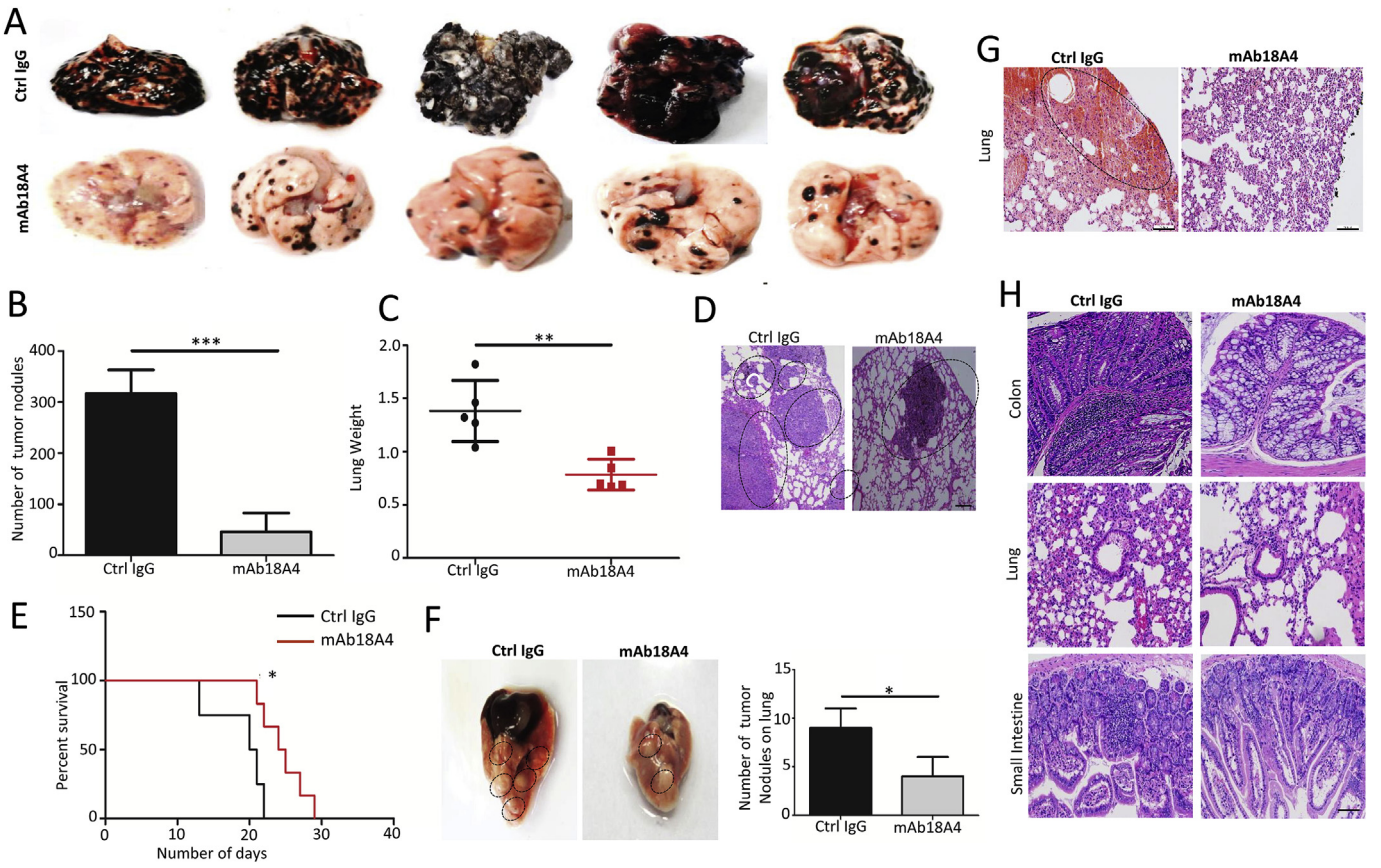

Fig. 4. mAb18A4 inhibits metastasis and prolongs survival span.(A) mAb18A4 inhibits B16F10 Melanoma lung metastasis. Mice were treated with 20 mg/kg mAb18A4 twice a week after two days of inoculation of B16F10 cells intravenously. The representative pictures of harvested lungs at the end of the experiment (21 days) are shown above with quantification data at bottom. **(B,C)** The number of pigmented tumors on the lung surface and the weight of the lungs was much less in mAb18A4 treated group than the control group respectively. **(D)** Representative H&E staining shows the histology of control group is not clear, congested and surrounded with micrometastases (demarcated with black dotted line), however the mAb18A4 treated mice lungs have lesser congestion and fewer densed areas (micro metastases). **(E)** mAb18A4 increased survival rate in pulmonary metastasis. All the Control IgG group mice died by the 22nd day but the mAb18A4 treated group survived till 29th day post tumor inoculation. **(F)** mAb18A4 suppreses lung metastasis in 4T1 breast adenocarcinoma model. Representative pictures of lungs harvested at the end of experiment. Quantification data of tumor nodules on lung is on the right. **(G)** Histological analysis revealed large areas of lung were metastasized with tumor cells in the control group (demarcated with black dotted line), whereas only few tumor cells could be seen in mAb18A4 treated lungs. **(H)** mAb18A4 inhibits spontaneous organ micro metastases in H460 tumor xenograft model. The organs were harvested at the end of experiment and stained with Haemotoxylin and Eosin (H&E) stain. mAb18A4 inhibited infiltration of tumor cells in Lung, Colon and Small Intestine. Quantification data are presented as mean ± SD (n = 5). Signals were quantified with GraphPad Prism. *, ** and *** indicate $P < 0.05$, $P < 0.02$, and $P < 0.001$ respectively as determined by an unpaired two tailed Student *t*-test. Scale bar 100 μm.

4. Discussion

AGR2 is intracellularly regulated in the ER and is secreted in the tumor microenvironment [46]. Several recent studies have elucidated the role of AGR2 in tumorigenesis and in the tumor microenvironment [46]. However, no potential targeted anti-AGR2 therapy is available at present. AGR2 is associated with drug resistance in breast cancer [47]. Recently, we reported that AGR2 mediates fulvestrant-induced drug resistance [9]. Therefore, we designed and developed a highly specific humanized monoclonal antibody mAb18A4 that binds to both human and mouse AGR2.

In the present study, we examined the effects of mAb18A4 against NSCLC growth and metastasis. Moreover, we examined the effects of mAb18A4 on tumor cell clonogenicity, proliferation, migration, and viability. We observed that mAb18A4 significantly inhibited AGR2-induced tumor characteristics *in vitro* and potently suppressed tumor progression in the xenograft tumor models. Moreover, mAb18A4 inhibited tumor metastasis in the various xenograft tumor models and increased the survival rate of the xenograft tumor models. Furthermore, we observed that regular treatment with mAb18A4 did not exert toxic effects on the major organs of the examined mice.

Experiments involving the xenograft tumor models showed that mAb18A4 inhibited the ERK1/2–MAPK pathway. Moreover, mAb18A4 significantly increased p53 and p21 expression levels in tumor tissues and tumor cells, which may be a possible mechanism through which mAb18A4 reduces tumor growth [18]. These results were consistent to the results of the *in vitro* experiments (Figs. 1E and 2E). Moreover, these results confirm the importance of AGR2 in the MAPK and p53 pathways. However, secretory AGR2 may also regulate other oncogenic pathways. For instance, we observed that both the A549 and H460 cell lines, which contain *KRAS* mutations [48], responded to mAb18A4.

A recent study reported that AGR2 promotes angiogenesis by directly interacting with VEGF-A, which increases VEGFR signaling and ultimately promotes metastasis. Another study reported that AGR2 inhibits the antitumor effect of bevacizumab, an anti-VEGF antibody [8]. These findings suggest that AGR2 is a potential therapeutic target or a predictive biomarker of angiogenesis. In the present study, mAb18A4 significantly reduced VEGF and CD31 expression in the xenograft tumor tissues, inhibited neovessel formation in the *ex vivo* mouse aortic ring assay, and inhibited tumor metastasis, thus confirming that mAb18A4 inhibits AGR2-induced angiogenesis and angiogenesis-dependent metastasis.

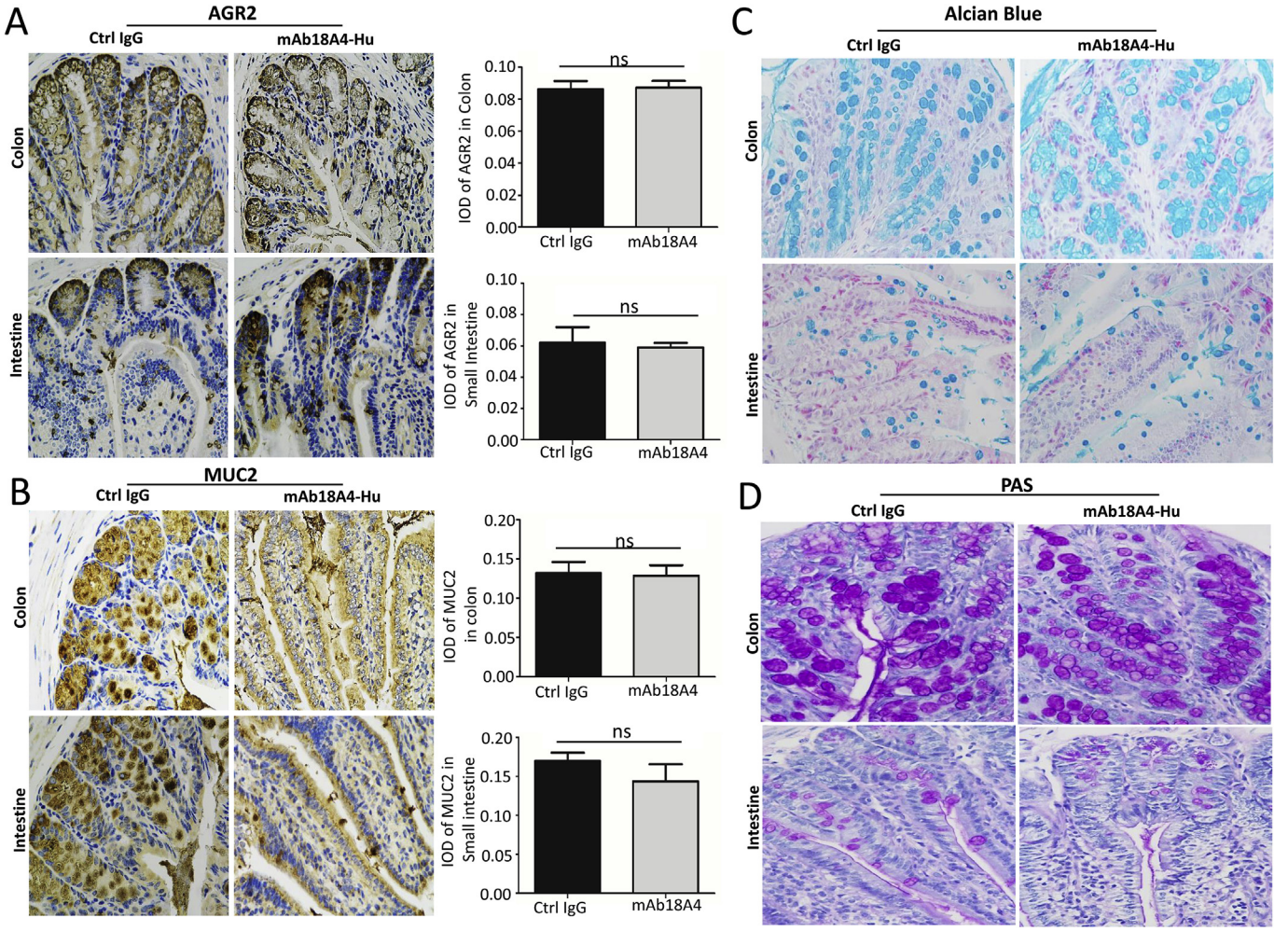

Fig. 5. mAb18A4-Hu has no adverse effect on mucin production in the intestine. Representative immunohistochemistry staining of AGR2 **(A)** and MUC2 **(B)** in colon and small intestine. AGR2 is essential for mucus and mucin production in the intestine. The mAb18A4-Hu treated group showed no significant adverse effect on AGR2 and MUC2 in Colon and Small intestine respectively. The Quantification data is presented on the bottom. **(C)** Representative images of Alcian Blue staining and **(D)** Periodic acid-Schiff (PAS) staining of Colon and Intestine. Scale bar, 50 μm. All quantification data above are presented as mean ± SEM. NS indicates not significant. Signals were quantified with Image J. (For interpretation of the references to colour in this figure legend, the reader is referred to the Web version of this article.)

Furthermore, mAb18A4 did not exert any treatment-related side effect in the treated mice. The results of the PK and toxicology analyses highlight the safety of mAb18A4 as a therapeutic agent. We observed that although mAb18A4 recognized and interacted with AGR2 in the intestine, colon, and lungs, which show *de novo* AGR2 expression, it did not exert harmful effects on these major organs or in blood. Moreover, our results suggest that mAb18A4 can be used as an antibody-based antigen diagnostic agent because it shows binding specificity.

In conclusion, the results of the present study indicate that AGR2 plays a vital role in tumor progression and metastasis. We developed a novel monoclonal antibody mAb18A4 for targeting AGR2, which is overexpressed in lung cancer as well as multiple other cancers. Our results showed that mAb18A4 induced tumor cell apoptosis, upregulated p53 expression, suppressed the ERK1/2–MAPK pathway, increased mouse survival, and inhibited AGR2-induced angiogenesis and metastasis.

Authors' contributions

Conception and design of the study: H. Negi, S. Kamle, D. Li, and Z. Wu.

Development of methodology: H. Negi, D.S. Mashausi, Z. Wu, and D. Li.

Acquisition of data (provision of animals, acquisition and management of patients, provision of facilities, etc.): H. Negi, S.B. Merugu, H.B. Mangukiya, B.Zhou, D.S. Mashausi, Q. Seher, F.N. Yunus, Z. Wu, and D. Li.

Analysis and interpretation of data (e.g., statistical, biostatistical, and computational analyses): H. Negi, S.B. Merugu, H.B. Mangukiya, Z. Li, and D. Li.

Writing, review, and/or revision of the manuscript: H. Negi, S.B. Merugu, Z. Li, S. Kamle, and D. Li.

Administrative, technical, or material support (i.e., reporting or organization of data and construction of databases): H. Negi, S.B. Merugu, Z. Wu, and D. Li.

Study supervision: Z. Wu and D. Li.

Grant support

This work was supported by grants from the National Natural Science Foundation of China (81373319, 81872790), Shanghai Science and Technology Commission Foundation (14431903400) and Shanghai International Science and Technology Cooperation Fund Project (184907411400).

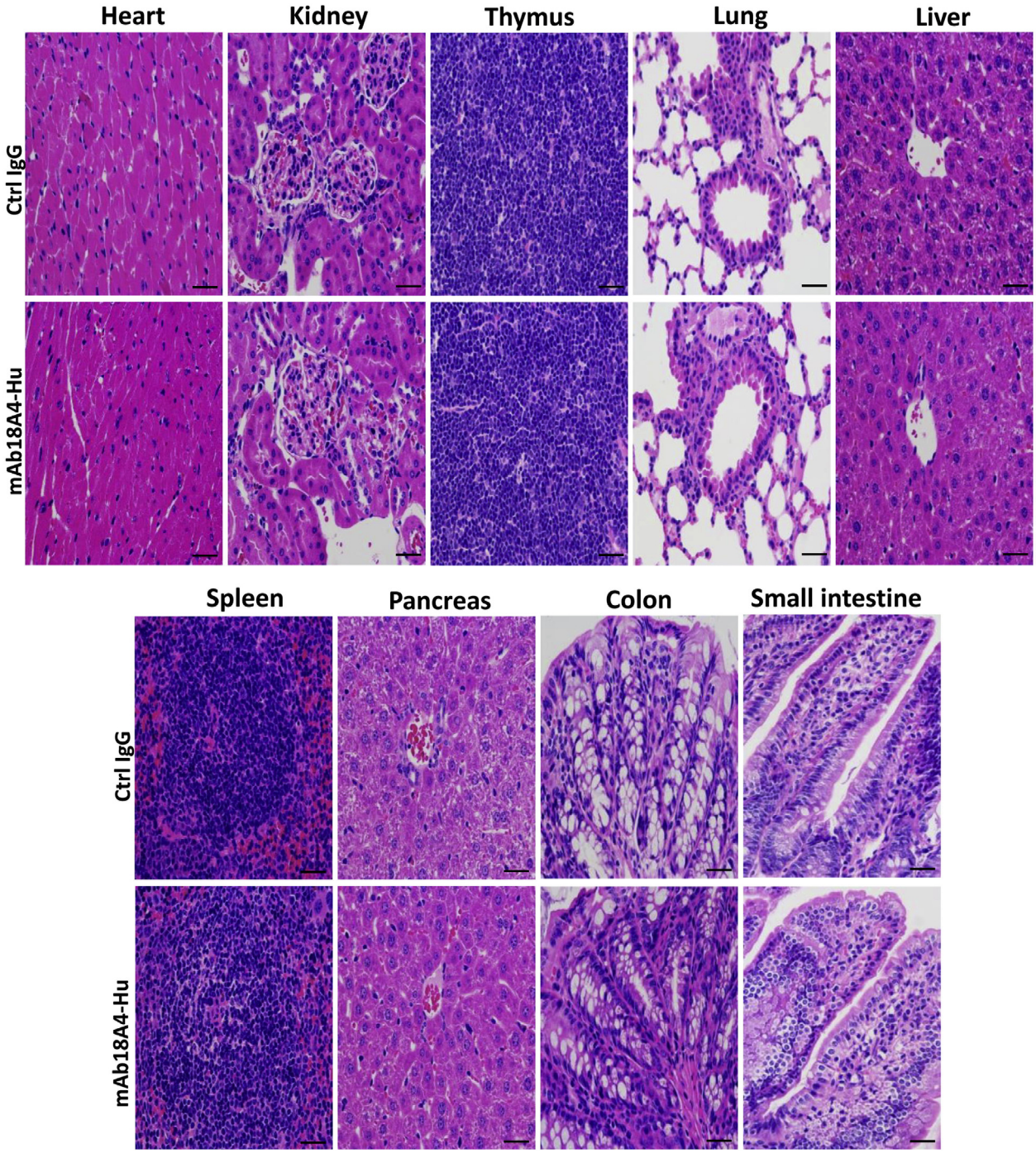

Fig. 6. Toxicology study of Humanized mAb18A4 on major Organs. Toxicology study was conducted in C57BL/6 mice treated 2 times a week for 5 weeks with 16 mg/kg humanized mAb18A4. At the end of the experiment, vital organs were harvested to be stained with Haemotoxylin & Eosin. Representative H&E pictures showing there was no significant toxicity found in vital organs. Scale bar 50 μm.

Disclosure of potential conflicts of interest

The authors declare that they do not have any conflicts of interest related to this study.

Acknowledgements

We thank Hao Liu, King's Laboratory, for performing the tail vein injections and Tianhong Yu and Jiawei Zhang for helping with mAb18A4 purification.

Appendix A. Supplementary data

Supplementary data to this article can be found online at https://doi.org/10.1016/j.canlet.2019.01.025.

References

[1] J.H. Bergstrom, K.A. Berg, A.M. Rodriguez-Pineiro, B. Stecher, M.E.V. Johansson, G.C. Hansson, AGR2, an endoplasmic reticulum protein, is secreted into the gastrointestinal mucus, PLoS One 9 (8) (2014) e104186.
[2] V. Brychtova, B. Vojtesek, R. Hrstka, Anterior gradient 2: a novel player in tumor cell biology, Cancer Lett. 304 (1) (2011) 1–7.

[3] E. Chevet, D. Fessart, F. Delom, A. Mulot, B. Vojtesek, R. Hrstka, et al., Emerging roles for the pro-oncogenic anterior gradient-2 in cancer development, Oncogene 32 (20) (2013) 2499–2509.

[4] Y. Li, W. Wang, Z. Liu, Y. Jiang, J. Lu, H. Xie, et al., AGR2 diagnostic value in nasopharyngeal carcinoma prognosis, Clin. Chim. Acta 484 (September 2018) 323–327.

[5] Z. Wang, Y. Hao, A.W. Lowe, The adenocarcinoma-associated antigen, AGR2, promotes tumor growth, cell migration, and cellular transformation, Cancer Res. 68 (2) (2008) 492–497.

[6] M.L. Salmans, F. Zhao, B. Andersen, The estrogen-regulated anterior gradient 2 (AGR2) protein in breast cancer: a potential drug target and biomarker, Breast Cancer Res. 15 (2) (2013) 204.

[7] S. Tian, J. Hu, K. Tao, J. Wang, Y. Chu, J. Li, et al., Secreted AGR2 promotes invasion of colorectal cancer cells via Wnt11-mediated non-canonical Wnt signaling, Exp. Cell Res. 364 (2) (2018) 198–207.

[8] M.Q. Jia, Y.X. Guo, D.Y. Zhu, N.Z. Zhang, L. Li, J. Jiang, et al., Pro-metastatic activity of AGR2 interrupts angiogenesis target bevacizumab efficiency via direct interaction with VEGFA and activation of NF-kappa B pathway, Bba-Mol Basis Dis 1864 (5) (2018) 1622–1633.

[9] Z.Q. Li, Q. Zhu, H. Chen, L.Y. Hu, H. Negi, Y. Zheng, et al., Binding of anterior gradient 2 and estrogen receptor-alpha: dual critical roles in enhancing fulvestrant resistance and IGF-1-induced tumorigenesis of breast cancer, Cancer Lett. 377 (1) (2016) 32–43.

[10] S.-B. Tian, K.-X. Tao, J. Hu, Z.-B. Liu, X.-L. Ding, Y.-N. Chu, et al., The prognostic value of AGR2 expression in solid tumours: a systematic review and meta-analysis, Sci Rep-Uk 7 (1) (2017) 15500.

[11] M. Alavi, V. Mah, E.L. Maresh, L. Bagryanova, S. Horvath, D. Chia, et al., High expression of AGR2 in lung cancer is predictive of poor survival, BMC Canc. 15 (2015) 655.

[12] E. Ondrouskova, L. Sommerova, R. Nenutil, O. Coufal, P. Bouchal, B. Vojtesek, et al., AGR2 associates with HER2 expression predicting poor outcome in subset of estrogen receptor negative breast cancer patients, Exp. Mol. Pathol. 102 (2) (2017) 280–283.

[13] T. Tsuji, R. Satoyoshi, N. Aiba, T. Kubo, K. Yanagihara, D. Maeda, et al., Agr2 mediates paracrine effects on stromal fibroblasts that promote invasion by gastric signet-ring carcinoma cells, Cancer Res. 75 (2) (2015) 356–366.

[14] H. Guo, Q. Zhu, X. Yu, S.B. Merugu, H.B. Mangukiya, N. Smith, et al., Tumor-secreted anterior gradient-2 binds to VEGF and FGF2 and enhances their activities by promoting their homodimerization, Oncogene 36 (36) (2017) 5098–5109.

[15] Z. Li, Z. Wu, H. Chen, Q. Zhu, G. Gao, L. Hu, et al., Induction of anterior gradient 2 (AGR2) plays a key role in insulin-like growth factor-1 (IGF-1)-induced breast cancer cell proliferation and migration, Med. Oncol. 32 (6) (2015) 577.

[16] Z.Q. Li, Q. Zhu, L.Y. Hu, H. Chen, Z.H. Wu, D.W. Li, Anterior gradient 2 is a binding stabilizer of hypoxia inducible factor-1 that enhances CoCl2-induced doxorubicin resistance in breast cancer cells, Cancer Sci. 106 (8) (2015) 1041–1049.

[17] T. Arumugam, D. Deng, L. Bover, H. Wang, C.D. Logsdon, V. Ramachandran, New blocking antibodies against novel AGR2-C4.4A pathway reduce growth and metastasis of pancreatic tumors and increase survival in mice, Mol. Canc. Therapeut. 14 (4) (2015) 941–951.

[18] R. Hrstka, P. Bouchalova, E. Michalova, E. Matoulkova, P. Muller, P.J. Coates, et al., AGR2 oncoprotein inhibits p38 MAPK and p53 activation through a DUSP10-mediated regulatory pathway, Mol Oncol 10 (5) (2016) 652–662.

[19] A. Ambolet-Camoit, L.C. Bui, S. Pierre, A. Chevallier, A. Marchand, X. Coumoul, et al., 2,3,7,8-Tetrachlorodibenzo-p-Dioxin counteracts the p53 response to a genotoxicant by upregulating expression of the metastasis marker AGR2 in the hepatocarcinoma cell line HepG2, Toxicol. Sci. 115 (2) (2010) 501–512.

[20] Q. Zhu, H.B. Mangukiya, D.S. Mashausi, H. Guo, H. Negi, S.B. Merugu, et al., Anterior gradient 2 is induced in cutaneous wound and promotes wound healing through its adhesion domain, FEBS J. 284 (17) (2017) 2856–2869.

[21] A. Gupta, A. Dong, A.W. Lowe, AGR2 gene function requires a unique endoplasmic reticulum localization motif, J. Biol. Chem. 287 (7) (2012) 4773–4782.

[22] S.-W. Park, G. Zhen, C. Verhaeghe, Y. Nakagami, L.T. Nguyenvu, A.J. Barczak, et al., The protein disulfide isomerase AGR2 is essential for production of intestinal mucus, P Natl Acad Sci USA 106 (17) (2009) 6950–6955.

[23] J. Malhotra, M. Malvezzi, E. Negri, C. La Vecchia, P. Boffetta, Risk factors for lung cancer worldwide, Eur. Respir. J. 48 (3) (2016) 889–902.

[24] X. Xue, X. Fei, W. Hou, Y. Zhang, L. Liu, R. Hu, miR-342-3p suppresses cell proliferation and migration by targeting AGR2 in non-small cell lung cancer, Cancer Lett. 412 (2018) 170–178.

[25] T.J. Lynch, D.W. Bell, R. Sordella, S. Gurubhagavatula, R.A. Okimoto, B.W. Brannigan, et al., Activating mutations in the epidermal growth factor receptor underlying responsiveness of non-small-cell lung cancer to gefitinib, N. Engl. J. Med. 350 (21) (2004) 2129–2139.

[26] D.A. Eberhard, B.E. Johnson, L.C. Amler, A.D. Goddard, S.L. Heldens, R.S. Herbst, et al., Mutations in the epidermal growth factor receptor and in KRAS are predictive and prognostic indicators in patients with non-small-cell lung cancer treated with chemotherapy alone and in combination with erlotinib, J. Clin. Oncol. 23 (25) (2005) 5900–5909.

[27] H. Lemjabbar-Alaoui, O.U. Hassan, Y.W. Yang, P. Buchanan, Lung cancer: biology and treatment options, Bba-Rev Cancer 1856 (2) (2015) 189–210.

[28] F.R. Fritzsche, E. Dahl, A. Dankof, M. Burkhardt, S. Pahl, I. Petersen, et al., Expression of AGR2 in non small cell lung cancer, Histol. Histopathol. 22 (7) (2007) 703–708.

[29] S. Narumi, Y. Miki, S. Hata, M. Ebina, M. Saito, K. Mori, et al., Anterior gradient 2 is correlated with EGFR mutation in lung adenocarcinoma tissues, Int. J. Biol. Markers 30 (2) (2015) E234–E242.

[30] H. Guo, H. Chen, Q. Zhu, X.Y. Yu, R. Rong, S.B. Merugu, et al., A humanized monoclonal antibody targeting secreted anterior gradient 2 effectively inhibits the xenograft tumor growth, Biochem Bioph Res Co 475 (1) (2016) 57–63.

[31] M. Baker, S.D. Robinson, T. Lechertier, P.R. Barber, B. Tavora, G. D'Amico, et al., Use of the mouse aortic ring assay to study angiogenesis, Nat. Protoc. 7 (1) (2012) 89–104.

[32] S. Tojkander, G. Gateva, P. Lappalainen, Actin stress fibers - assembly, dynamics and biological roles, J. Cell Sci. 125 (8) (2012) 1855–1864.

[33] L. Sommerova, E. Ondrouskova, B. Vojtesek, R. Hrstka, Suppression of AGR2 in a TGF-beta-induced Smad regulatory pathway mediates epithelial-mesenchymal transition, BMC Canc. 17 (1) (2017) 546.

[34] G. Pearson, F. Robinson, T.B. Gibson, B.E. Xu, M. Karandikar, K. Berman, et al., Mitogen-activated protein (MAP) kinase pathways: regulation and physiological functions, Endocr. Rev. 22 (2) (2001) 153–183.

[35] V. Brychtova, A. Mohtar, B. Vojtesek, T.R. Hupp, Mechanisms of anterior gradient-2 regulation and function in cancer, Semin. Canc. Biol. 33 (2015) 16–24.

[36] E. Cerami, J. Gao, U. Dogrusoz, B.E. Gross, S.O. Sumer, B.A. Aksoy, The cBio cancer genomics portal: an open platform for exploring multidimensional cancer genomics data (vol 2, pg 401, 2012), Cancer Discov. 2 (10) (2012) 960.

[37] J. Gao, B.A. Aksoy, U. Dogrusoz, G. Dresdner, B. Gross, S.O. Sumer, et al., Integrative analysis of complex cancer genomics and clinical profiles using the cBioPortal, Sci. Signal. 6 (269) (2013) pl1.

[38] L. Dumartin, H.J. Whiteman, M.E. Weeks, D. Hariharan, B. Dmitrovic, C.A. Iacobuzio-Donahue, et al., AGR2 is a novel surface antigen that promotes the dissemination of pancreatic cancer cells through regulation of cathepsins B and D, Cancer Res. 71 (22) (2011) 7091–7102.

[39] C. Clarke, P. Rudland, R. Barraclough, The metastasis-inducing protein AGR2 is O-glycosylated upon secretion from mammary epithelial cells, Mol. Cell. Biochem. 408 (1–2) (2015) 245–252.

[40] H.E. Innes, D. Liu, R. Barraclough, M.P.A. Davies, P.A. O'Neill, A. Platt-Higgins, et al., Significance of the metastasis-inducing protein AGR2 for outcome in hormonally treated breast cancer patients, Br. J. Canc. 94 (7) (2006) 1057–1065.

[41] R. Liu, X. Li, W. Gao, Y. Zhou, S. Wey, S.K. Mitra, et al., Monoclonal antibody against cell surface GRP78 as a novel agent in suppressing PI3K/AKT signaling, tumor growth, and metastasis, Clin. Canc. Res. 19 (24) (2013) 6802–6811.

[42] L.L. Bao, A. Haque, K. Jackson, S. Hazari, K. Moroz, R. Jetly, et al., Increased expression of P-glycoprotein is associated with doxorubicin chemoresistance in the metastatic 4T1 breast cancer model, Am. J. Pathol. 178 (2) (2011) 838–852.

[43] J. Zhang, Y. Jin, S. Xu, J. Zheng, Q.I. Zhang, Y. Wang, et al., AGR2 is associated with gastric cancer progression and poor survival, Oncol Lett 11 (3) (2016) 2075–2083.

[44] K. Kozaki, K. Koshikawa, Y. Tatematsu, O. Miyaishi, H. Saito, T. Hida, et al., Multifaceted analyses of a highly metastatic human lung cancer cell line NCI-H460-LNM35 suggest mimicry of inflammatory cells in metastasis, Oncogene 20 (31) (2001) 4228–4234.

[45] J. Perez-Vilar, R.L. Hill, The structure and assembly of secreted mucins, J. Biol. Chem. 274 (45) (1999) 31751–31754.

[46] D. Fessart, C. Domblides, T. Avril, L.A. Eriksson, H. Begueret, R. Pineau, et al., Secretion of protein disulphide isomerase AGR2 confers tumorigenic properties, Elife 5 (2016).

[47] R. Hrstka, J. Podhorec, R. Nenutil, L. Sommerova, J. Obacz, M. Durech, et al., Tamoxifen-dependent induction of AGR2 is associated with increased aggressiveness of endometrial cancer cells, Canc. Invest. 35 (5) (2017) 313–324.

[48] Y.K. Yoon, H.P. Kim, S.W. Han, D.Y. Oh, S.A. Im, Y.J. Bang, et al., KRAS mutant lung cancer cells are differentially responsive to MEK inhibitor due to AKT or STAT3 activation: implication for combinatorial approach, Mol. Carcinog. 49 (4) (2010) 353–362.